Sensitivity analysis of the superposition model to characterise the fibre bridging effect on the mode I Paris curve

Monticeli, F.M.; Biagini, D.; Mosleh, Yasmine; Pascoe, J.A.

Publication date
2025

Document Version
Final published version

Published in
28th ABCM International Congress of Mechanical Engineering

Citation (APA)
Monticeli, F. M., Biagini, D., Mosleh, Y., & Pascoe, J. A. (2025). Sensitivity analysis of the superposition model to characterise the fibre bridging effect on the mode I Paris curve. In *28th ABCM International Congress of Mechanical Engineering* (pp. 1). Article COB-2025-0400 ABCM, Brazilian Society of Mechanical Sciences and Engineering.

COBEM 2025
28TH INTERNATIONAL CONGRESS OF MECHANICAL ENGINEERING
ABCM Brazilian Society of Mechanical Sciences and Engineering
28th ABCM International Congress of Mechanical Engineering
November 09-11, 2025, Curitiba-PR, Brazil

COB-2025-0400
SENSITIVITY ANALYSIS OF THE SUPERPOSITION MODEL TO CHARACTERISE THE FIBRE BRIDGING EFFECT ON THE MODE I PARIS CURVE

Francisco Maciel Monticeli
Department of Aerospace Structures and Materials, Faculty of Aerospace Engineering, Delft University of Technology, Kluyverweg 1, 2629 HS Delft, the Netherlands, *f.m.monticeli@tudelft.nl*

Davide Biagini
Department of Aerospace Structures and Materials, Faculty of Aerospace Engineering, Delft University of Technology, Kluyverweg 1, 2629 HS Delft, the Netherlands, *d.biagini-1@tudelft.nl*

Yasmine Mosleh
Department of Engineering Structures, Faculty of Civil Engineering and Geosciences, Delft University of Technology, Stevinweg 1, 2628 CN Delft, the Netherlands, *y.mosleh@tudelft.nl*

John-Alan Pascoe
Department of Aerospace Structures and Materials, Faculty of Aerospace Engineering, Delft University of Technology, Kluyverweg 1, 2629 HS Delft, the Netherlands, *j.a.pascoe@tudelft.nl*

Abstract. *Fibre bridging in laminated composites has a significant effect on Mode I delamination behaviour, resulting in improved opening resistance and altered fatigue crack growth rates. This study investigates the sensitivity of a recently developed superposition model to capture monotonic and cyclic bridging contributions to fatigue delamination. Double cantilever beam (DCB) specimens were tested under quasi-static and cyclic loading to derive R-curves and bridging stress profiles. A set of eleven different parameter combinations were used to generate zero-bridging Paris curves, followed by ANOVA based sensitivity analysis. The results show that the fracture toughness parameters G0 (initiation) and Gs (saturation) have the strongest influence on the Paris parameter coefficients, while the maximum end-opening δ* plays a secondary role. Heat map-based analysis shows that larger differences between G_0 and Gs lead to stronger bridging effects and more conservative fatigue curves. This framework provides valuable insight into data-driven calibration of bridging models and supports application-specific fatigue design strategies.*

Keywords: *CFRP, Fatigue delamination, Fibre bridging, Sensitivity analysis*

1. INTRODUCTION

Delamination under cyclic loading remains a critical failure mechanism in carbon fibre reinforced polymers (CFRPs), particularly in aerospace and other advanced structures subjected to long-term fatigue (Ding et al., 2021; Kumar et al., 2024; Li et al., 2024). Mode I delamination, characterised by opening crack growth, is particularly affected by mechanisms that contribute to energy dissipation or provide crack tip shielding, such as fibre bridging (Khan et al., 2014). The bridging phenomenon introduces additional complexity to fatigue modelling due to its non-linear nature (Yao et al., 2017).

Fibre bridging occurs when intact fibres span a delaminated interface, creating a bridging stress that resists further crack propagation. This results in an apparent increase in fracture toughness, as captured by *R-curves*, and has a significant impact on the fatigue behaviour of composite laminates (Sørensen and Jacobsen, 1998). While beneficial in slowing crack growth, fibre bridging makes it difficult to characterise the intrinsic material properties as it masks the true crack-tip behaviour (Ben Gur and Banks-Sills, 2024).

Several approaches have been proposed to account for fibre bridging, including the use of bridging laws, cohesive zone models and analytical corrections (Erives et al., 2023; Joosten et al., 2022; Tian et al., 2023). Among these, a recently proposed superposition model provides a simple and efficient method to separate the contributions of monotonic and cyclic bridging (Monticeli et al., 2025). By relying on experimentally derived *R-curves* and end-opening measurements, this model provides an interpretable framework for reconstructing the intrinsic Paris curve free of bridging effects.

However, the model relies on several key parameters such as fracture toughness at zero bridging (G_0), at saturation level (G_s) and end-opening (δ^*). These parameters are intrinsically variable due to experimental scatter, fitting procedures, and data post-processing assumptions. Understanding the sensitivity of the model to these inputs is essential to ensure reliable application of the proposed model in structural design.

The objective of this study is to quantify the sensitivity of the superposition model to variations in fibre bridging parameters and to assess how these affect the prediction of Mode I Paris curve behaviour in carbon fibre composites. By combining experimental data, statistical tools and fatigue modelling, this work provides insight into the reliability of bridging corrections and suggests guidelines for the selection of conservative or nominal fatigue curves based on material characterisation.

2. MATERIALS AND METHODS

Composite laminates were manufactured using 24 layers of IM7/8552 unidirectional carbon fibre prepreg (Hexcel®). Curing was performed in an autoclave at 120 °C for 2 h followed by 180 °C for 4 h, 0.2 bar vacuum and 7 bar pressure.

Mode I quasi-static and fatigue tests were performed based on a double cantilever beam (DCB) specimen, using a 500 N MTS servo-hydraulic machine applying a displacement-controlled load at 2.5 Hz with a load ratio of 0.1 (Figure 1a). The quasi-static test was performed at 1 mm/min. Specimens were cut on a diamond blade saw to the following dimensions 160 × 25 × 3 mm³ according to ASTM D5528, 2014 (Figure 1b). A PTFE film was inserted as a 50 mm initial crack. Crack growth was tracked using sequential imaging (every 100-1000 cycles) and post-processing using *ImageJ*. The end-opening displacement (δ^*) near the fibre bridging zone was measured from the images (Figure 1c).

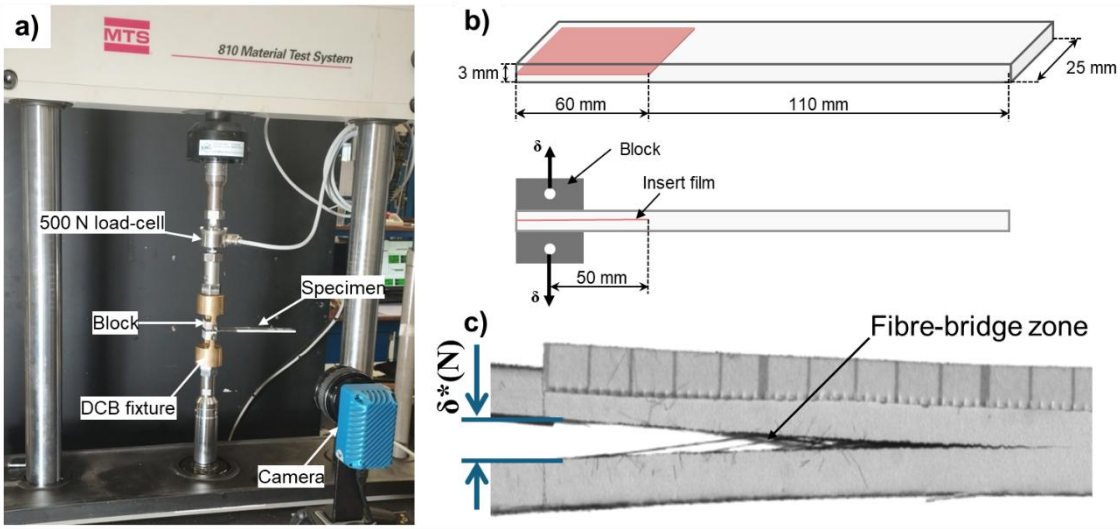

Figure 1. Illustration of a) DCB set-up fixture in fatigue machine, b) specimen dimensions and c) fibre bridging zone and end-opening (δ*).

3. MODELLING FIBRE-BRIDGING CONTRIBUTION

The strain energy release rate (SERR) was calculated using the modified compliance calibration method (ASTM D5528). Starting from a quasi-static loading regime, the resulting *R-curve* – relating fracture toughness (G_r) to crack extension (a-a_0) – shows an initial increase followed by a steady-state plateau (G_s) (Yao et al., 2018). The increasing part reflects the development of fibre bridging, while the plateau indicates saturation of this mechanism. Sørensen et al. (Sørensen and Jacobsen, 1998) proposed the formulation of Eq. (1) to estimate the fibre bridging stress (FB stress) in Mode I intralaminar crack growth, based on the difference (G_s-G_0) divided by the end opening at the bridging region.

$$G_r = G_0 + \int_0^{\delta^*} \sigma(\delta^*) d\delta^*, \qquad \sigma(\delta^*) = \frac{\partial G_r}{\partial \delta^*} \tag{1}$$

where, G_r is the crack opening resistance, G_0 is the fracture toughness at zero-bridging, δ^* is the end-opening in the fibre bridging region, and $\sigma(\delta^*)$ is the fibre bridging stress at the given end-opening. Note: the maximal end-opening represents the bridging saturation level (where G_r becomes equal to G_s).

By tracking compliance changes under cyclic loading, it is possible to quantify the separate contributions of the fibre bridging generated during quasi-static pre-cracking and that generated during fatigue propagation. By individual integration, the fibre bridging energy from pre-cracking ($G_{FBZ,mono}$) is defined in Eq. (2). The additional cyclic contribution ($G_{FBZ,cyclic}$), described in Eq. (3), results from increasing end-opening levels due to crack propagation,

which increases the bridging density. The sum of these two components gives the superposition model Eq. (4), described in more detail in Ref. Monticeli et al., 2025.

$$G_{FBZ,mono} = \int_{\delta^*_{min}}^{\delta^*_{QS}} \sigma(\delta^*) d\delta^* \text{, for } \delta^* > \delta^*_{min} \tag{2}$$

$$G_{FBZ,cyclic} = \int_{\delta^*_{QS}}^{\delta^*_{max}} \sigma(\delta^*) d\delta^* = \left(2\sigma_{QS}\sqrt{\delta^*_{QS}}\right)\left(\sqrt{\delta^*(N)} - \sqrt{\delta^*_{QS}}\right) \tag{3}$$

$$G_{FBZ,total} = G_{FBZ,mono} + G_{FBZ,cyclic} \tag{4}$$

where, δ^*_{QS} represents the end-opening for pre-crack formation (quasi-static), $\delta^*(N)$ is the end-opening for given cycle (N), δ^*_{min} is the minimal measurement of end-opening close to crack tip, σ_{QS} is the fibre bridging stress, and $G_{FBZ,i}$ represents the strain energy related to the fibre bridging zone for initial quasi-static monotonic loading and for cyclic loading.

3.1 RELEVANT MODEL PARAMETERS FOR SENSITIVITY STUDY

The main source of variability in the proposed superposition model lies in the estimation of the fibre bridging stress, which directly affects the representation of the fatigue behaviour. Consequently, any uncertainty in the determination of the fibre bridging stress will inevitably affect the accuracy of the model in Eq. (4).

The first source of variability is the determination of G_0 (the strain energy release rate without fibre bridging). This can be estimated by polynomial fitting of the *R-curve* and extrapolating to zero crack extension, resulting in a projected G_0 value (Figure 2a). For the first G_0 values, two polynomial curves of 2nd and 3rd order were fitted. Alternatively, G_0 can be derived from the fibre bridging stress curve by linearly connecting the peak bridging stress to the origin (zero opening) as shown in Figure 2b. The FB stress curve is represented by an exponential decay as a function of end-opening, with the peak value measured experimentally by visual analysis of the crack opening. If a boundary condition factor is considered where fibre bridging occurs linearly from peak to zero end-opening, additional energy is added to the curve (red area in Figure 2b). The additional area under the linear fitting represents the additional storage energy from fibre bridging, that can be subtracted from G_r to derive the zero bridging fracture toughness (G_0).

A second major variability arises in the determination of G_s (the steady-state fracture toughness) which depends on: (*i*) the interpretation of the saturation region, and (*ii*) the intrinsic scatter or repeatability of the experimental data (Figure 2a). The chosen value of G_s also influences the corresponding crack length at which saturation is assumed, and consequently the associated maximum end-opening displacement. All these parameters are derived by data analysis rather than visual identification of the fibre bridging zone to reduce subjectivity. To determine G_s, three conditions were applied in the region of maximum saturation: the first takes into account the maximum value of G_r (Max G_s), the second the average value of the saturation region (Average G_s) and the third the minimum value of the saturation region (Min G_s).

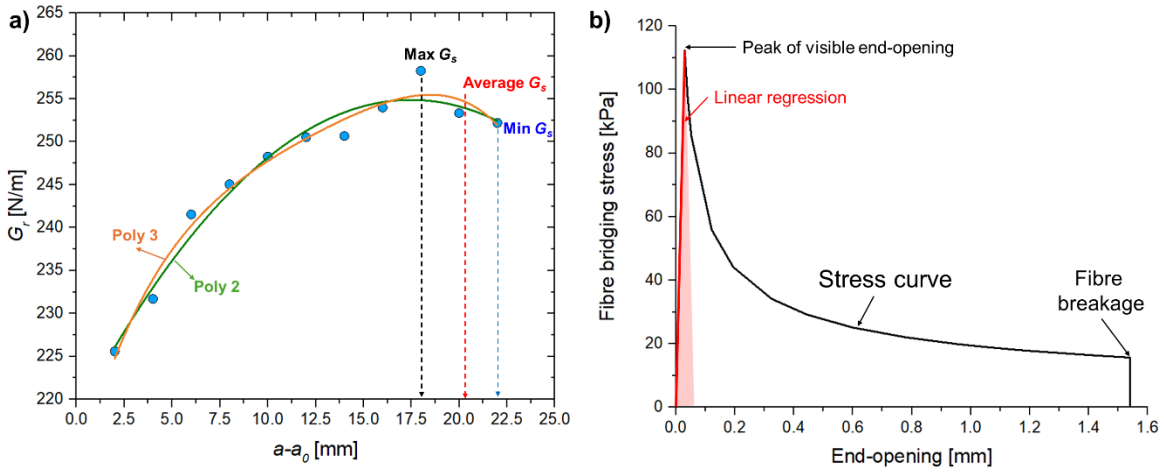

Figure 2. Illustration of a) *R-curve* and parameter determination, and b) linearisation of maximal stress to minimal end-opening. Note: Poly 2 – 2nd polynomial order fitting, Poly 3 – 3rd polynomial order fitting, Max G_s – maximal value of G_r (at the saturation region), and Min G_s – minimal value of G_r (at the saturation region).

4. RESULTS AND DISCUSSION

4.1 QUASI-STATIC REGIME

This section presents the results from the quasi-static regime where key parameters were identified. Tests were carried out on five specimens to assess repeatability in determining zero bridging fracture toughness, saturation SERR and maximum end opening. Figure 3a shows the *R-curve*, highlighting the inherent variability between specimens. An initial increase in Gr is observed due to the development of fibre bridging, followed by a plateau indicating saturation. The observed variation of approximately ±10 N/m reflects differences in the onset of fibre bridging and saturation behaviour.

The bridging stress profile was derived from the *R-curve* data for the five specimens using Eq. (1), but with 11 variations on the data analysis procedure, labelled Experiment I - XI. The variations arise from the choices made in obtaining G_0 and G_s values. As explained above, G_0 can be obtained by fitting either a 2nd or 3rd order polynomial to the *R-curve* (Figure 3a) or by linear extrapolation from the peak bridging stress. G_s can be determined based on the maximum Gr value in the saturation region, the minimum G_r value, or the average G_r value (Figure 3a)

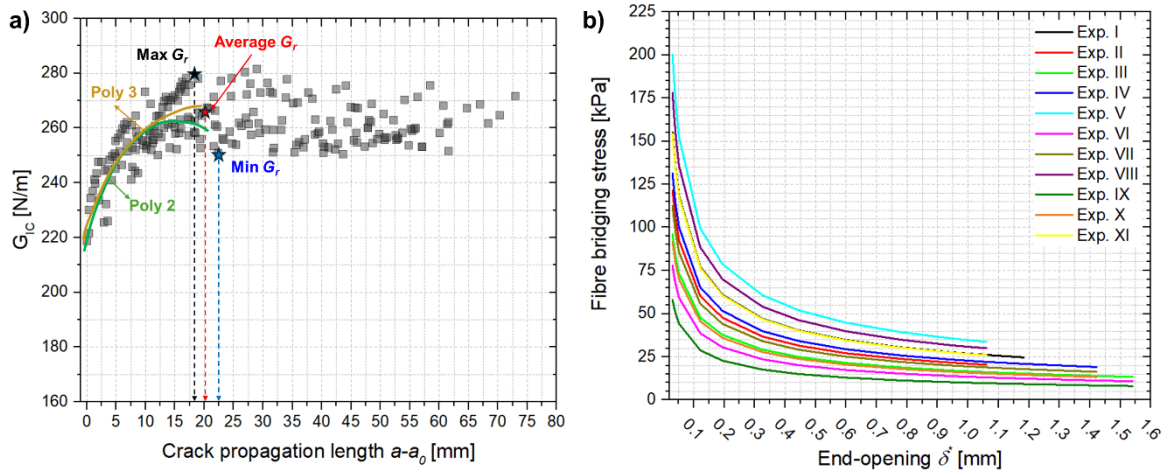

Figure 3. a) Experimental *R-curve* and b) Fibre bridging stress for different parameter.

Table 1 summarises the effects of the different experiments on the *R-curve* analysis. It presents the calculated G_0 values obtained from second and third order polynomial fitting or linear extrapolation of the bridging stress curve based on the maximum measured point. In addition, the table shows the minimum, maximum and mean values of G_s, reflecting the intrinsic variability and repeatability of the tests. The corresponding end opening values associated with each variation in G_s are also given.

Figure 3b illustrates the resulting FB stress evolution: starting from a high stress near the crack tip, the fibre bridging stress decreases with opening until δ^*_{max} is reached – at this point, the fibres begin to fail and the bridging stress drops to zero. In the plot, a considerable variability can be observed in the peak stress (i.e. the left side limit of the different lines), the curve slope, the maximum opening (i.e. right-side limit of the different curves). As this bridging stress profile is used to calculate both monotonic and cyclic contributions to fatigue, similar variability is expected in the resulting fatigue curves.

Polynomial interpolation of the *R-curve* was used to determine the parameters G_0, G_s and end opening value (Table 1 Exp. I and II). Those three values are particularly relevant as it allows the complete definition of the fibre bridging (FB) stress curve. Conversely, the determination of G_s was also approached by analysing the saturation region of the *R-curve* and extracting three different values - maximum, minimum and average - based on the variability observed in repeated tests. Using these G_s values with the experimentally G_{IC} obtained from visual measurement to construct different previous FB stress curves. The energy contribution from fibre bridging was estimated by calculating the area between the maximum stress point and the zero end-opening value, by linear fitting. By subtracting this additional bridging energy from the original G_{IC}, three corresponding values of G_0 were derived, one for each case of G_s (max, average, min). Subsequently, combinations of different G_s and G_0 values (experimental conditions III to XI) were analysed to evaluate the sensitivity and variability in determining the FB stress curve parameters and consequently their influence on the resulting Paris Law behaviour. The end-opening values were always derived as a function of the corresponding G_s used in each configuration.

Table 1. Variable parameters for determining fibre bridging stress.

Method	**Experiment Nº**	G_0 **[N/m]**	G_s **[N/m]**	δ^* **[mm]**
Poly 2nd interpolation	I	218.30	276.67	1.18
Poly 3rd interpolation	II	215.71	256.90	0.96
Regression minimal FB stress / Minimal G_r	III	208.70	250.04	1.54
Regression minimal FB stress / Average G_r	IV	208.70	262.97	1.42
Regression minimal FB stress / Maximal G_r	V	208.70	280.11	1.06
Regression average FB stress / Minimal G_r	VI	216.60	250.04	1.54
Regression average FB stress / Average G_r	VII	216.60	262.97	1.42
Regression average FB stress / Maximal G_r	VIII	216.60	280.11	1.06
Regression maximal FB stress / Minimal G_r	IX	225.13	250.04	1.54
Regression maximal FB stress / Average G_r	X	225.13	262.97	1.42
Regression maximal FB stress / Maximal G_r	XI	225.13	250.04	1.54

4.2 FATIGUE REGIME

This section presents the experimental Paris curve for Mode I fatigue delamination and the application of the superposition model to characterise fibre bridging effects under cyclic loading. Figure 4a shows the experimental Paris curve plotted as crack propagation rate (da/dN) versus G_{max}, which is used here as the similarity parameter. The Paris law was fitted in the linear regime $(da/dN) = C(G_{max})^n$. Data scatter is due to the 7-point method (ASTM E647) used to calculate crack growth rates.

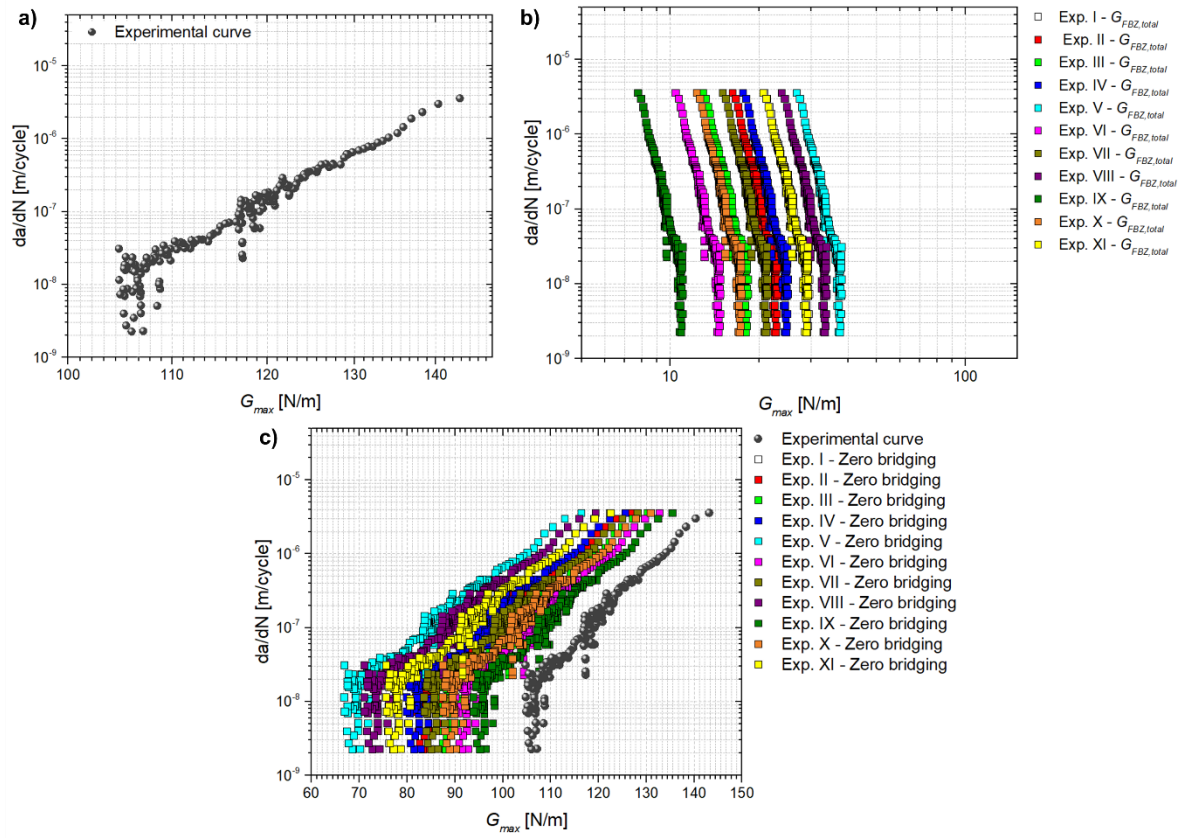

Figure 4. a) Experimental Paris curve, b) Total SERR of fibre bridging ($G_{FBZ,total}$), and c) zero bridging curves for each FB stress.

Using the bridging stress curves (Figure 2b) and the superposition model Eq. (4), each experimental point was corrected to account for fibre bridging. A progressive increase in G with da/dN is observed in Figure 4b, reflecting the accumulation of strain energy due to bridging: initially from quasi-static pre-cracking and subsequently from cyclic propagation. This energy storage explains the shift in the experimental curve. A major advantage of the model is that it preserves the experimental variability in the predicted results.

Figure 4b presents the different fibre bridging contributions calculated based on the different FB stress profiles of the different experiments. The curves shows that the use of different fibre bridging parameters results in a clear horizontal shift in SERR values. Although the slope also varies considerably between experiments, this variability is less perceptible in the plot because of the overlap among the individual curves. The magnitude of the fatigue energy storage is directly related to the bridging stress profile, highlighting the need for accurate characterisation of this parameter to isolate monotonic and cyclic contributions. The observed variability highlights the sensitivity of the method to data quality and bridging curve definition.

By characterising the cyclic bridging effect, a zero-bridging Paris curve can be reconstructed by subtracting the total bridging energy ($G_{FBZ,total}$) from each G_{max} value (Figure 4c). This correction allows for a more conservative representation of crack tip behaviour, excluding fibre bridging effects (Banks-Sills and Gur, 2024). The corrected curves show a shift towards lower energy release rates (monotonic contribution) and a decrease in slope (cyclic contribution), reflecting the reduced stiffness caused by fibre bridging (Monticeli et al., 2025). Due to the high variability in the bridging stress curves, the zero bridging curves also show considerable scatter. In all cases, a reduction in strain energy (in terms of Paris law coefficient C and slope n) is observed.

Table 2 summarises the Paris law fitting results for both the experimental curve and the zero bridging curves derived from each test, based on the fibre bridging parameters listed in Table 1. The experimental curve has a steep slope (n = 18.98) and an extremely low *intercept-C*, reflecting the combined effect of intrinsic crack growth and fibre bridging. In contrast, the zero bridging models show significantly lower slopes and higher C values, isolating the intrinsic delamination behaviour.

Given the variability observed in experiments I-XI, it is difficult to define a single 'true' curve. However, this variability also provides flexibility: the selection of a representative curve can be tailored to the required level of conservatism. For example, in safety critical structures where crack arrest by fibre bridging is unlikely - either because bridging is minimal by design or because there are no strengthening mechanisms - a lower slope (e.g. Exp. V) may

represent a lower-bound scenario. Conversely, curves with a higher slope (e.g. Exp. IX) may be useful in assessing upper performance limits where fibre bridging plays a significant role in crack retardation.

Interestingly, the shape and positioning of the zero bridging curves suggest that fibre bridging not only contributes to energy dissipation but also stabilises crack growth. This finding highlights the dual role of fibre bridging - both as a strengthening mechanism and as a source of interpretation complexity - and emphasises the need for application-specific fatigue modelling strategies.

Table 2. Paris fitting parameter for experimental and each zero bridging curves.

Paris curve	***C* [m/cycle]**	**Slope - *n***
Experimental	5.13×10^{-47}	18.98
Exp. I – zero bridging	2.21×10^{-31}	12.06
Exp. II – zero bridging	3.12×10^{-34}	13.33
Exp. III – zero bridging	1.56×10^{-36}	14.36
Exp. IV – zero bridging	2.37×10^{-33}	12.94
Exp. V – zero bridging	6.06×10^{-28}	10.51
Exp. VI – zero bridging	2.56×10^{-38}	15.15
Exp. VII – zero bridging	4.87×10^{-35}	13.69
Exp. VIII – zero bridging	1.39×10^{-29}	11.25
Exp. IX – zero bridging	2.37×10^{-40}	16.05
Exp. X – zero bridging	5.81×10^{-37}	14.55
Exp. XI – zero bridging	1.85×10^{-31}	12.09

4.3 SENSITIVITY ANALYSIS

The variability observed in the experimental data raises an important question: which parameter in the fibre bridging stress curve has the most significant influence on the predicted zero-bridging Paris curves? To address this, statistical models were applied to quantify the individual contributions of each input variable from Table 1 - namely G_0, G_s and δ^* - to the Paris law parameters C and n listed in Table 2. An analysis of variance (ANOVA) was performed, and the results are summarised in Table 3. To improve numerical stability, the response C was analysed in logarithmic form (-*Log C*).

In all cases, high *F-values* and *p-values* well below 0.05 confirm that the null hypothesis can be rejected and that all three factors significantly influence both C and n. Sensitivity was assessed based on the percentage of the total sum of squares, indicating the relative contribution of each factor. Consistently, G_s showed the strongest influence (≈59%), followed by G_0 (≈34%), with δ^* contributing the least (≈7%). This lower sensitivity of δ^* can be attributed to its dependence on the choice of G_s, making it a secondary factor in the model.

These results suggest that the zero-bridging Paris behaviour is predominantly affected by the fracture toughness parameters G_0 and G_s, reinforcing their critical role in accurately modelling fatigue delamination when fibre bridging effects are removed.

Table 3. Analysis of variance of factors effect on Paris parameter as response.

Slope *n*			
Factor	***F-value***	***p-value***	***Sensitivity (%)***
G_0	2383.64	3.96×10^{-10}	33.68%
G_s	4179.05	5.57×10^{-11}	59.05%
δ^*	514.65	8.19×10^{-08}	7.27%
- Log (*C*)			
Factor	***F-value***	***p-value***	***Sensitivity (%)***
G_0	2444.54	3.62×10^{-10}	33.74%
G_s	4274.61	5.15×10^{-11}	59.00%
δ^*	525.63	7.61×10^{-08}	7.26%

As G_0 and G_s were identified as the most influential parameters, a sensitivity analysis was performed using the heat maps in Table 4. This analysis examines how the combined variation of these two factors affects the reduction in the Paris law parameters n and C. Again, the values of $-Log\ C$ were used to simplify the calculations of compliance variation between experiments. The horizontal axis represents G_0 values, the vertical axis represents G_s experimental levels, and the colour scale indicates the percentage reduction relative to the original experimental values, added in the table as reference values.

Table 4. Sensitivity analysis of G_0 and G_s on Paris parameters for zero bridging curve.

Slope *n* Ref.: 18.98		***G₀* [N/m]**				
		208.70	**215.71**	**216.60**	**218.30**	**225.13**
***Gₛ* [N/m]**	**250.04**	24%	16%	20%	15%	15%
	256.90	24%	30%	20%	19%	14%
	262.97	32%	24%	28%	23%	23%
	276.67	36%	34%	33%	36%	27%
	280.11	45%	36%	41%	35%	36%
- Log (C) = 46.28 Ref.: 5.13 x 10^{-47}		***G₀* [N/m]**				
		208.70	215.71	216.60	218.30	225.13
***Gₛ* [N/m]**	**250.04**	23%	21%	19%	20%	14%
	256.90	28%	28%	25%	24%	19%
	262.97	30%	28%	26%	27%	22%
	276.67	39%	37%	37%	34%	32%
	280.11	41%	39%	38%	38%	34%

A clear trend is observed for both parameters: larger reductions in n and $-Log\ C$ occur when high values of G_s are combined with low values of G_0. This result reflects the larger gap between initial and saturated fracture toughness, which corresponds to a higher fibre bridging density in the *R-curve*. Thus, the identification of high G_s values, even within the experimental variability, results in a more pronounced bridging correction and leads to more conservative Paris curves.

This analysis also provides a practical strategy for tailoring fatigue predictions. By selectively selecting input parameters based on bridging potential, designers can construct bounds for damage tolerance design. For example, scenarios with high G_s and low G_0 can serve as upper-bound models that capture maximal bridging effects, while combinations with smaller $G_s - G_0$ gaps can represent more realistic or nominal fatigue behaviour. This approach strengthens the link between fracture characterisation and predictive modelling.

5. CONCLUSIONS

This work presents a comprehensive sensitivity analysis of a superposition model used to characterise fibre bridging effects in Mode I delamination under fatigue loading. By combining experimental *R-curve* data, bridging stress formulations and Paris model fitting, the study isolates the influence of bridging on fatigue crack growth rates. The results clearly demonstrate that the fracture toughness parameters, G_0 and G_s, play a central role in the correction of Paris curve, while the influence of δ^* showed a secondary contribution. Through ANOVA and visual heat map analysis, the work quantifies how variability in the input parameters propagates into the zero bridging Paris curve, allowing designers to interpret and limit the effect of fibre bridging. Moreover, the results also highlight the potential of this approach in the selection of conservative/optimistic fatigue models, depending on the structural application. By enabling the prediction of zero-bridging Paris curve, the method allows the isolation of intrinsic crack-tip behaviour, which is essential for damage tolerance assessment. The framework developed strengthens the link between experimental characterisation and predictive modelling, contributing to more robust fatigue design methodologies for composite structures.

6. ACKNOWLEDGEMENTS

The research was funded by the European Union under GA No. 101091409 (D-STANDART). Views and opinions expressed are however those of the author(s) only and do not necessarily reflect those of the European Union. Neither the European Union nor the granting authority can be held responsible for them.

7. DATA AVAILABILITY

The data underlying this work is publicly available via a Zenodo repository: 10.5281/zenodo.14831359

8. REFERENCES

ASTM D5528, 2014. Standard test method for mode I interlaminar fracture toughness of unidirectional fiber-reinforced polymer matrix composites. Am. Stand. Test. Methods 03, 1–12. https://doi.org/10.1520/D5528

Banks-Sills, L., Gur, H. Ben, 2024. The effect of fiber bridging on mode I fatigue delamination propagation—part I: Testing. Fatigue Fract. Eng. Mater. Struct. 1–17. https://doi.org/10.1111/ffe.14362

Ben Gur, H., Banks-Sills, L., 2024. The effect of fiber bridging on mode I fatigue delamination propagation—Part II: Cohesive zone model. Fatigue Fract. Eng. Mater. Struct. 3529–3545. https://doi.org/10.1111/ffe.14382

Ding, J., Cheng, L., Chen, X., Chen, C., Liu, K., 2021. A review on ultra-high cycle fatigue of CFRP. Compos. Struct. 256, 113058. https://doi.org/10.1016/j.compstruct.2020.113058

Erives, R., Sørensen, B.F., Goutianos, S., 2023. Extraction of mix-mode cohesive laws of a unidirectional composite undergoing delamination with large-scale fibre bridging. Compos. Part A Appl. Sci. Manuf. 165, 107346. https://doi.org/10.1016/j.compositesa.2022.107346

Joosten, M.W., Dávila, C.G., Yang, Q., 2022. Predicting fatigue damage in composites subjected to general loading conditions. Compos. Part A Appl. Sci. Manuf. 156. https://doi.org/10.1016/j.compositesa.2022.106862

Khan, R., Alderliesten, R., Benedictus, R., 2014. Two-parameter model for delamination growth under mode I fatigue loading (Part B : Model development) 65, 201–210.

Kumar, V., Bedi, R., Kumar, M., 2024. The fatigue of carbon fiber reinforced polymer composites – A review. Mater. Today Proc. https://doi.org/10.1016/j.matpr.2024.06.004

Li, X., Monticeli, F., Pascoe, J.A., Mosleh, Y., 2024. Interlaminar fracture behaviour of emerging laminated-pultruded CFRP plates for wind turbine blades. Eng. Fract. Mech. 308. https://doi.org/10.1016/j.engfracmech.2024.110353

Monticeli, F.M., Biagini, D., Mosleh, Y., Pascoe, J.A., 2025. A novel analytical model to characterise the monotonic and cyclic contribution of fibre bridging during Mode I fatigue delamination in (C)FRPs. Compos. Part B Eng. 297, 112319. https://doi.org/10.1016/j.compositesb.2025.112319

Sørensen, B.F., Jacobsen, T.K., 1998. Large-scale bridging in composites: R-curves and bridging laws. Compos. Part A Appl. Sci. Manuf. 29, 1443–1451. https://doi.org/10.1016/S1359-835X(98)00025-6

Tian, D., Gong, Y., Gao, Y., Zou, L., Zhang, J., Zhao, L., Hu, N., 2023. Numerical modelling of the mode I fracture behavior in composite laminates with significant R-curve effect. Theor. Appl. Fract. Mech. 128, 104172. https://doi.org/10.1016/j.tafmec.2023.104172

Yao, L., Cui, H., Sun, Y., Guo, L., Chen, X., Zhao, M., Alderliesten, R.C., 2018. Fibre-bridged fatigue delamination in multidirectional composite laminates. Compos. Part A Appl. Sci. Manuf. 115, 175–186. https://doi.org/10.1016/j.compositesa.2018.09.027

Yao, L., Sun, Y., Guo, L., Zhao, M., Jia, L., Alderliesten, R.C., Benedictus, R., 2017. A modified Paris relation for fatigue delamination with fibre bridging in composite laminates. Compos. Struct. 176, 556–564. https://doi.org/10.1016/j.compstruct.2017.05.070

9. RESPONSIBILITY NOTICE

The authors are the only responsible for the printed material included in this paper.